Optimal Selection of Piezoelectric Substrates and Crystal Cuts for SAW-Based Pressure and Temperature Sensors

Xiangwen Zhang, Fei-Yue Wang, *Fellow, IEEE*, and Li Li, *Member, IEEE*

***Abstract*—In this paper, the perturbation method is used to study the velocity shift of surface acoustic waves (SAW) caused by surface pressure and temperature variations of piezoelectric substrates. Effects of pressures and temperatures on elastic, piezoelectric, and dielectric constants of piezoelectric substrates are fully considered as well as the initial stresses and boundary conditions. First, frequency pressure/temperature coefficients are introduced to reflect the relationship between the SAW resonant frequency and the pressure/temperature of the piezoelectric substrates. Second, delay pressure/temperature coefficients are introduced to reflect the relationship among the SAW delay time/phase and SAW delay line-based sensors' pressure and temperature. An objective function for performance evaluation of piezoelectric substrates is then defined in terms of their effective SAW coupling coefficients, power flow angles (PFA), acoustic propagation losses, and pressure and temperature coefficients. Finally, optimal selections of piezoelectric substrates and crystal cuts for SAW-based pressure, temperature, and pressure/temperature sensors are derived by calculating the corresponding objective function values among the range of X-cut, Y-cut, Z-cut, and rotated Y-cut quartz, lithium niobate, and lithium tantalate crystals in different propagation directions.**

I. Introduction

A surface acoustic wave (SAW) is a kind of acoustic wave that propagates along a surface of an elastic substrate and whose amplitude decays exponentially with substrate depth. Since its velocity is smaller than that of electromagnetic waves and it has a high quality factor and low loss at high frequencies, a SAW is now widely used in filters, resonators, delay lines, and other signal processing devices. Quartz, lithium niobate ($LiNbO_3$), and lithium tantalate ($LiTaO_3$) crystals are three frequently used piezoelectric substrates for SAW devices. The acoustic characteristics of a substrate surface vary with the variation of pressure and temperature over it, i.e., the bias of piezoelectric crystal elastic, piezoelectric, and dielectric constants and the shift of the SAW velocity, which result in changes of the SAW resonant frequency, delay time, and phase. Thus, measurement of the pressure and temperature on the substrate surface can be transformed to measure the shift of resonant frequency for SAW resonators or delay time and phase for SAW delay lines.

Recently, several pressure and temperature sensors based on SAW resonators or delay lines have been produced [1]. The SAW sensor is small, light, reliable, stable, passive, and sensitive. In addition, the SAW sensor can work under poor environmental conditions, such as closed chambers, or moving and rotating parts of engines [1]–[8]. In 1996, Pohl and Seifert at the University of Technology in Vienna designed a wireless passive SAW pressure sensor based on a SAW delay line and used it to measure the pressure in a vehicle tire [4], [5]. Buff *et al.* in Germany designed a wireless passive SAW sensor, using two SAW resonators with different frequencies, to measure the tire pressure by comparing the frequency difference of the two resonators. This sensor shows better performance in precision, and will not be affected by movement or rotation [6], [7]. In 1998, Steindle *et al.* developed the SAW hybrid sensor using the combination of the SAW delay line and conventional pressure sensors [8]. Recently, the authors developed a pressure/temperature sensor based on two identical SAW delay lines on both sides of the substrate to measure the tire pressure and temperature simultaneously [1].

The selection of piezoelectric substrates and crystal cuts is an important problem in SAW sensor design. Using different piezoelectric substrates and crystal cuts, the SAW sensors will have different performance. Thus, it is necessary to select the optimal substrate and crystal cut which yields the best performance for the SAW sensor. In 1970, Schulz *et al.* studied the temperature dependence of SAW velocity on α-quartz [9]. In 1980, Sinha and Tiersten analyzed the same problem using perturbation method [10]. In 1992, Ballandras and Bigler studied the SAW devices with low sensitivity to mechanical and thermoelastic stresses using the perturbation and finite element methods [11]. In 1995, Taziev *et al.* studied the pressure-sensitive cuts for SAW in α-quartz [12]. In 2000, Ma and Shi studied the temperature-sensitive cuts for SAW in quartz [13].

Manuscript received March 27, 2005; accepted January 15, 2007. This work was supported in part by the Chinese NNSF 60334020 and 60621001, 973 Project 2006CB705506 and 2002CB312200. In addition, it was part of the triangle intelligent tires project supported by CASIC, INC., and Triangle Tire Co., Ltd.

X. Zhang is with the Key Laboratory for Complex Systems and Intelligence Science, Chinese Academy of Sciences, Beijing, China, and the Department of Computer Science and Technology, Guilin University of Electronic Technology, Guilin, China.

F.-Y. Wang is with the Key Laboratory for Complex Systems and Intelligence Science, Chinese Academy of Sciences, Beijing, China, and the Program for Advanced Research in Complex Systems, Department of Systems and Industrial Engineering, University of Arizona, Tucson, AZ (e-mail: feiyue@sie.arizona.edu).

L. Li is with the Department of Automation, Tsinghua University, Beijing, China.

Digital Object Identifier 10.1109/TUFFC.2007.374

However, they only considered the bias of the second-order elastic constants of quartz caused by the pressure or temperature perturbation, and the SAW velocity or frequency shift caused by the bias of elastic constants for the SAW resonator. In fact, the piezoelectric and dielectric constants are also affected by the perturbation simultaneously, which will result in the shift in SAW velocity or frequency of the SAW resonator. For SAW pressure and temperature sensors based on SAW delay lines, the shift of the delay time or phase caused by the pressure and temperature bias is a meaningful factor in this sensor design. In addition, the effective SAW coupling coefficient, the power flow angle (PFA), and the acoustic propagation loss also affect the performance of piezoelectric substrates. They should not be neglected in the selection of piezoelectric substrates and crystal cuts for SAW sensors.

In this paper, the SAW velocity shift caused by the pressure and temperature bias on the substrate surface is first analyzed in Section II using the perturbation method. The boundary conditions of the free space and the bias of the second-order elastic constants, and the piezoelectric and dielectric constants caused by pressure and temperature variations are also considered. In Section III, the pressure and temperature frequency coefficients of piezoelectric substrates with respect to the SAW resonator frequency shift, pressure, and temperature are defined. In Section IV, the relationships among the effective SAW coupling coefficient, PFA, acoustic propagation loss, and the performance of the piezoelectric substrates are explained. In Section V, an objective function for optimal selection of piezoelectric substrates and crystal cuts for SAW-based pressure and temperature sensors is defined. By solving the objective function in terms of the range of X-cut, Y-cut, Z-cut, and rotated Y-cut quartz, $LiNbO_3$, and $LiTaO_3$ crystals in different propagation directions, the optimal selections of piezoelectric substrates and crystal cuts are finally achieved in Section VI.

II. SAW Velocity Shift Caused by Temperature and Pressure Perturbation

Generally, the linear electroelastic equations for SAW piezoelectric substrates are written as [14], [15]:

$$K_{L\gamma,L} = \rho^0 \ddot{u}_\gamma, \; D_{L,L} = 0, \tag{1}$$

$$K_{L\gamma} = c_{L\gamma Ma} u_{a,M} + e_{ML\gamma} \varphi_{,M}, \tag{2}$$

$$D_L = e_{LMa} u_{a,M} - \varepsilon_{LM} \varphi_{,M}, \tag{3}$$

where (1) is the stress equation of motion and the charge equation of electrostatics. Eq. (2) is the linear piezoelectric constitutive equation. The terms $K_{L\gamma}$, u_γ, and D_L denote the components of stress, mechanical displacement, and electric displacement, respectively; ρ^0 and φ denote the mass density and electric potential, respectively; $c_{L\gamma Ma}$ and ε_{LM} are the elastic and dielectric constants, respectively; and $e_{ML\gamma}$ and $e_{LM\alpha}$ are the piezoelectric constants.

In (1)–(3) and the following equations in this paper, a convention is employed that a comma followed by an index denotes partial differentiation regarding a space coordinate, the dot notation for differentiation with respect to time, and the summation convention for repeated tensor indices.

The linear electroelastic equations for small fields superposed on a bias may be written as [14], [15]:

$$\widetilde{K}_{L\gamma,L} = \rho^0 \ddot{\tilde{u}}_\gamma, \;\; D_{L,L} = 0, \tag{4}$$

$$\begin{aligned} \widetilde{K}_{L\gamma} &= (c_{L\gamma Ma} + \hat{c}_{L\gamma Ma})\, \tilde{u}_{a,M} + (e_{ML\gamma} + \hat{e}_{ML\gamma})\, \tilde{\varphi}_{,M} \\ &= (c_{L\gamma Ma} \tilde{u}_{a,M} + e_{ML\gamma} \tilde{\varphi}_{,M}) \\ &\quad + (\hat{c}_{L\gamma Ma} \tilde{u}_{a,M} + \hat{e}_{ML\gamma} \tilde{\varphi}_{,M}) \\ &= \widetilde{K}^0_{L\gamma} + \widetilde{K}^P_{L\gamma}, \end{aligned} \tag{5}$$

$$\begin{aligned} \widetilde{D}_L &= (e_{LMa} + \hat{e}_{LMa})\, \tilde{u}_{a,M} - (\varepsilon_{LM} + \hat{\varepsilon}_{LM})\, \tilde{\varphi}_{,M} \\ &= (\hat{e}_{LMa} \tilde{u}_{a,M} - \hat{\varepsilon}_{LM} \tilde{\varphi}_{,M}) + (\hat{e}_{LMa} \tilde{u}_{a,M} - \hat{\varepsilon}_{LM} \tilde{\varphi}_{,M}) \\ &= \widetilde{D}^0_L + \widetilde{D}^P_L, \end{aligned} \tag{6}$$

where

$$\begin{aligned} \hat{c}_{L\gamma Ma} &= T_{LM} \delta_{\gamma a} + c_{L\gamma MaAB} E_{AB} + c_{L\gamma KM} \hat{u}_{a,K} \\ &\quad + c_{LKMa} \hat{u}_{\gamma,K} - k_{AL\gamma Ma} \hat{\varphi}_{,A} \\ &\quad + g_{L\gamma Ma} + \frac{dc_{L\gamma Ma}}{dT}(T - T_0), \end{aligned} \tag{7}$$

$$\begin{aligned} \hat{e}_{ML\gamma} &= -k_{ML\gamma BC} E_{BC} - e_{MLK} \hat{u}_{\gamma,K} - b_{AML\gamma} \hat{\varphi}_{,A} \\ &\quad + g_{ML\gamma} + \frac{de_{ML\gamma}}{dT}(T - T_0), \end{aligned} \tag{8}$$

$$\begin{aligned} \hat{\varepsilon}_{LM} &= b_{LMCD} E_{CD} - \chi_{LMC} \hat{\varphi}_{,C} \\ &\quad - 2\varepsilon_0 E_{ML} + \frac{d\varepsilon_{LM}}{dT}(T - T_0), \end{aligned} \tag{9}$$

$$\begin{aligned} g_{L\gamma Ma} &= \varepsilon_0 (E_\xi E_\xi (\delta_{M\gamma} \delta_{La} - \delta_{Ma} \delta_{L\gamma}) \\ &\quad + E_\gamma E_\beta (\delta_{L\beta} \delta_{Ma} - \delta_{M\beta} \delta_{La}) \\ &\quad + E_a E_\beta (\delta_{M\beta} \delta_{L\gamma} - \delta_{L\beta} \delta_{M\gamma})), \end{aligned} \tag{10}$$

$$g_{ML\gamma} = \varepsilon_0 (E_\beta \delta_{M\beta} \delta_{L\gamma} - E_\gamma \delta_{La} \delta_{Ma} - E_a \delta_{La} \delta_{M\gamma}). \tag{11}$$

Eq. (4) constitute the stress equation of motion and the charge equation of electrostatics referred to the reference (or undeformed) coordinate axes fixed in the solid. Eq. (5)–(6) are the linear electroelastic constitutive equations. The terms $\widetilde{K}_{L\gamma}$, $\tilde{u}_\gamma$, and $\widetilde{D}_L$ are the components of the small field Piola-Kirchhoff stress tensor, reference mechanical displacement, and electric displacement vector, respectively; $\tilde{\varphi}$ denotes the reference small field electric potential; $\hat{c}_{L\gamma Ma}$ and $\hat{\varepsilon}_{LM}$ denote the bias of the elastic and dielectric constants in the small field perturbation, respectively; $\hat{e}_{ML\gamma}$ and $\hat{e}_{LM\alpha}$ denote the bias of the piezoelectric constants in the small field perturbation; $\widetilde{K}^0_{L\gamma}$ and $\widetilde{D}^0_L$ denote the reference static stress tensor and electric displacement vector, respectively; $\widetilde{K}^P_{L\gamma}$ and $\widetilde{D}^P_L$ denote the bias of the small field Piola-Kirchhoff stress tensor and the reference electric displacement vector, respectively; $\hat{\varphi}$ denotes the reference small field electric potential bias; $\hat{u}_a$ denotes the bias of the small field mechanical displacement; $c_{L\gamma MaAB}$, $b_{AML\gamma}$, χ_{LMC}, and $k_{ML\gamma BC}$ denote the third-order elastic, electrostrictive, electric permeability,

and electro-elastic constants, respectively; ε_0 is the dielectric constant in the atmosphere; and T_0 and T are the temperatures in the primary state and present state.

Let T_{LM}, E_{AB}, and E_j denote the components of the static biasing stress, strain, and electric field, respectively. This will lead to

$$T_{LM} = c_{LMRS}\hat{u}_{R,S} + e_{RLM}\hat{\varphi}_{,M}, \tag{12}$$

$$E_{AB} = \frac{\hat{u}_{A,B} + \hat{u}_{B,A}}{2}, \tag{13}$$

$$E_j = -\frac{\partial\hat{\varphi}}{\partial a_j}. \tag{14}$$

In the rest of this paper, we assume that u_γ and φ have a time dependence of $e^{j\omega_0 t}$, $\tilde{u}_\gamma$ and $\tilde{\varphi}$ have a time dependence of $e^{j\omega t}$, and ω_0 and ω represent the circular frequencies of SAW propagation in the primary state and present state, respectively. From (1) and (4), we obtain

$$\begin{aligned}&\left(K_{L\gamma,L} - \rho^0\ddot{u}_\gamma\right)\tilde{u}_\gamma - \left(\widetilde{K}_{L\gamma,L} - \rho^0\ddot{\tilde{u}}_\gamma\right)u_\gamma \\ &= \left(K_{L\gamma,L} + \rho^0\omega_0^2 u_\gamma\right)\tilde{u}_\gamma - \left(\widetilde{K}_{L\gamma,L} + \rho^0\omega^2\tilde{u}_\gamma\right)u_\gamma = 0.\end{aligned} \tag{15}$$

From (15) and (5), we have

$$\begin{aligned}\rho^0(\omega^2 - \omega_0^2)u_\gamma\tilde{u}_\gamma &= K_{L\gamma,L}\tilde{u}_\gamma - \widetilde{K}_{L\gamma,L}u_\gamma \\ &= K_{L\gamma,L}\tilde{u}_\gamma - \widetilde{K}^0_{L\gamma,L}u_\gamma - \widetilde{K}^P_{L\gamma,L}u_\gamma,\end{aligned} \tag{16}$$

$$\begin{aligned}K_{L\gamma,L}\tilde{u}_\gamma - \widetilde{K}^0_{L\gamma,L}u_\gamma &= \left(K_{L\gamma}\tilde{u}_\gamma\right)_{,L} - K_{L\gamma}\tilde{u}_{\gamma,L} \\ &\quad - \left(\left(\widetilde{K}^0_{L\gamma}u_\gamma\right)_{,L} - \widetilde{K}^0_{L\gamma}u_{\gamma,L}\right) \\ &= \left(K_{L\gamma}\tilde{u}_\gamma - \widetilde{K}^0_{L\gamma}u_\gamma\right)_{,L} + \widetilde{K}^0_{L\gamma}u_{\gamma,L} - K_{L\gamma}\tilde{u}_{\gamma,L}.\end{aligned} \tag{17}$$

From (1)–(6), considered the symmetry of elastic, piezoelectric, and dielectric constants, we obtain

$$\begin{aligned}&\widetilde{K}^0_{L\gamma}u_{\gamma,L} - K_{L\gamma}\tilde{u}_{\gamma,L} = \left(c_{L\gamma Ma}\tilde{u}_{a,M} + e_{ML\gamma}\tilde{\varphi}_{,M}\right)u_{\gamma,L} \\ &\quad - \left(c_{L\gamma Ma}u_{a,M} + e_{ML\gamma}\varphi_{,M}\right)\tilde{u}_{\gamma,L} = e_{ML\gamma}\tilde{\varphi}_{,M}u_{\gamma,L} \\ &\quad - e_{ML\gamma}\varphi_{,M}\tilde{u}_{\gamma,L} = \left(D_M + \varepsilon_{ML}\varphi_{,L}\right)\tilde{\varphi}_{,M} \\ &\quad - \left(\widetilde{D}^0_M + \varepsilon_{ML}\tilde{\varphi}_{,L}\right)\varphi_{,M} = D_M\tilde{\varphi}_{,M} - \widetilde{D}^0_M\varphi_{,M} \\ &= \left(D_M\tilde{\varphi}\right)_{,M} - D_{M,M}\tilde{\varphi} - \left(\left(\widetilde{D}^0_M\varphi\right)_{,M} - \widetilde{D}^0_{M,M}\varphi\right) \\ &\quad = \left(D_M\tilde{\varphi} - \widetilde{D}^0_M\varphi\right)_{,M} + \widetilde{D}^0_{M,M}\varphi \\ &\quad = \left(D_M\tilde{\varphi} - \widetilde{D}^0_M\varphi\right)_{,M} - \widetilde{D}^P_{M,M}\varphi.\end{aligned} \tag{18}$$

Notice that the repeated tensor indices obey the summation convention; the result will not change when the suffix M is replaced by L. According to this consideration, (18) may be written as

$$\widetilde{K}^0_{L\gamma}u_{\gamma,L} - K_{L\gamma}\tilde{u}_{\gamma,L} = \left(D_L\tilde{\varphi} - \widetilde{D}^0_L\varphi\right)_{,L} - \widetilde{D}^P_{L,L}\varphi. \tag{19}$$

From (16)–(19), this leads to

$$\begin{aligned}\rho^0(\omega^2 - \omega_0^2)u_\gamma\tilde{u}_\gamma &= \left(K_{L\gamma}\tilde{u}_\gamma - \widetilde{K}^0_{L\gamma}u_\gamma\right)_{,L} \\ &\quad + \left(D_L\tilde{\varphi} - \widetilde{D}^0_L\varphi\right)_{,L} - \widetilde{D}^P_{L,L}\varphi - \widetilde{K}^P_{L\gamma,L}u_\gamma.\end{aligned} \tag{20}$$

Considering the periodicity variation of u_γ and $\tilde{u}_\gamma$, we discuss the condition in one wavelength λ and the u_γ and $\tilde{u}_\gamma$ change in a reference volume V_0, which is one wavelength long, one unit wide, and infinitely thick. By integration of both sides of (20) over the reference volume V_0 and based on the divergence theorem, we get

$$\begin{aligned}H = \int_{V_0}\rho^0(\omega^2 - \omega_0^2)\tilde{u}_\gamma u_\gamma dV &= \int_{S_0} N_L\big(K_{L\gamma}\tilde{u}_\gamma - \widetilde{K}^0_{L\gamma}u_\gamma \\ &\quad + D_L\tilde{\varphi} - \widetilde{D}^0_L\varphi\big)dS - \int_{V_0}\left(\widetilde{D}^P_{L,L}\varphi + \widetilde{K}^P_{L\gamma,L}u_\gamma\right)dV,\end{aligned} \tag{21}$$

where S_0 denotes the reference surface area enclosing the reference volume V_0, and N_L denotes the unit normal to the reference position of the surface.

Before perturbation, the substrate surface is traction-free and abuts free space, so the boundary conditions are

$$N_L K_{L\gamma} = 0, \tag{22}$$

$$N_L D_L + N_L\varepsilon_0\varphi_{,L} = 0. \tag{23}$$

If there is perturbation from temperature and pressure, the substrate surface abuts free space and is subjected to traction $\overline{T}_\gamma$ per unit reference area. The boundary conditions are

$$N_L\left(\widetilde{K}^0_{L\gamma} + \widetilde{K}^P_{L\gamma}\right) = \overline{T}_\gamma, \tag{24}$$

$$N_L\left(\widetilde{D}^0_L + \widetilde{D}^P_L\right) + N_L\varepsilon_0\tilde{\varphi}_{,L} = 0. \tag{25}$$

From (21)–(25), this leads to

$$\begin{aligned}H &= \int_{S_0} N_L\left(\widetilde{K}^P_{L\gamma}u_\gamma + \widetilde{D}^P_L\varphi + \varepsilon_0\left(\tilde{\varphi}_{,L}\varphi - \varphi_{,L}\tilde{\varphi}\right)\right)dS \\ &\quad - \int_{S_0}\overline{T}_\gamma u_\gamma dS = \int_{V_0}\left(\widetilde{D}^P_{L,L}\varphi + \widetilde{K}^P_{L\gamma,L}u_\gamma\right)dV \\ &\quad = \int_{S_0} N_L\varepsilon_0\left(\tilde{\varphi}_{,L}\varphi - \varphi_{,L}\tilde{\varphi}\right)dS - \int_{S_0}\overline{T}_\gamma u_\gamma dS \\ &\quad + \int_{V_0}\left(\widetilde{K}^P_{L\gamma}u_\gamma + \widetilde{D}^P_L\varphi\right)_{,L}dV - \int_{V_0}\left(\widetilde{D}^P_{L,L}\varphi + \widetilde{K}^P_{L\gamma,L}u_\gamma\right)dV \\ &\quad = \int_{S_0} N_L\varepsilon_0\left(\tilde{\varphi}_{,L}\varphi - \varphi_{,L}\tilde{\varphi}\right)dS - \int_{S_0}\overline{T}_\gamma u_\gamma dS \\ &\quad + \int_{V_0}\left(\widetilde{D}^P_L\varphi_{,L} + \widetilde{K}^P_{L\gamma}u_{\gamma,L}\right)dV.\end{aligned} \tag{26}$$

In the substrate surface, φ and $\tilde{\varphi}$ should satisfy Laplace's equation as

$$\varphi_{,LL} = 0, \tag{27}$$

$$\tilde{\varphi}_{,LL} = 0. \tag{28}$$

From (27)–(28), we have

$$\int_{S_0} N_L \varepsilon_0 \left(\tilde{\varphi}_{,L}\varphi - \varphi_{,L}\tilde{\varphi}\right) dS = \int_{V_0} \varepsilon_0 \left(\tilde{\varphi}_{,L}\varphi - \varphi_{,L}\tilde{\varphi}\right)_{,L} dV = \int_{V_0} \varepsilon_0 \left(\tilde{\varphi}_{,LL}\varphi - \varphi_{,LL}\tilde{\varphi}\right) dV = 0. \quad (29)$$

From (26) and (29), we have

$$H = \int_{V_0} \left(\widetilde{D}_L^P \varphi_{,L} + \widetilde{K}_{L\gamma}^P u_{\gamma,L}\right) dV - \int_{S_0} \overline{T}_\gamma u_\gamma dS. \quad (30)$$

From (5)–(6), (30) can be further expressed as

$$\begin{aligned} H = &\int_{V_0} \left(\hat{e}_{LMa}\tilde{u}_{a,M} - \hat{\varepsilon}_{LM}\tilde{\varphi}_{,M}\right)\varphi_{,L} dV - \int_{S_0} \overline{T}_\gamma u_\gamma dS \\ &+ \int_{V_0} \left(\hat{c}_{L\gamma Ma}\tilde{u}_{a,M} + \hat{e}_{ML\gamma}\tilde{\varphi}_{,M}\right) U_{\gamma,L} dV \\ = &\hat{c}_{L\gamma Ma} \int_{V_0} \tilde{u}_{a,M} u_{\gamma,L} dV + \hat{e}_{ML\gamma} \int_{V_0} \tilde{\varphi}_{,M} u_{\gamma,L} dV \\ &+ \hat{e}_{LMa} \int_{V_0} \tilde{u}_{a,M}\varphi_{,L} dV - \hat{\varepsilon}_{LM} \int_{V_0} \tilde{\varphi}_{,M}\varphi_{,L} dV - \int_{S_0} \overline{T}_\gamma u_\gamma dS. \end{aligned} \quad (31)$$

For the small field perturbation, it can be assumed that $\Delta = \omega - \omega_0$, $|\Delta| \ll \omega_0$, and

$$H = 2\rho^0 \Delta\omega_0 \int_{V_0} \tilde{u}_\gamma u_\gamma dV, \quad (32)$$

$$\Delta = \frac{H}{2\rho^0 \omega_0 \int_{V_0} \tilde{u}_\gamma u_\gamma dV}. \quad (33)$$

Suppose the SAW wavelength λ is a constant; then it leads to $\Delta = \omega - \omega_0 = 2\pi(v - v_0)/\lambda$, where v_0 and v are the SAW velocities on the substrate surface in the primary state and present state, respectively. The SAW velocity shift should be

$$\frac{\Delta v}{v_0} = \frac{v - v_0}{v_0} = \frac{\Delta}{\omega_0} = \frac{H}{2\rho^0 \omega_0^2 \int_{V_0} \tilde{u}_\gamma u_\gamma dV}. \quad (34)$$

Suppose the SAW propagates in the x_1-direction and there is no attenuation in the x_2-direction. The SAW propagating solution satisfying (1)–(3) and the boundary conditions (22)–(23) of piezoelectric substrates can be written as

$$u_\gamma = \sum_{m=1}^{4} C^{(m)} A_\gamma^{(m)} e^{\{j[\omega_0 t - \xi(x_1 + p^{(m)} x_3)]\}}, \quad (35)$$

$$\varphi = \sum_{m=1}^{4} C^{(m)} B^{(m)} e^{\{j[\omega_0 t - \xi(x_1 + p^{(m)} x_3)]\}}, \quad (36)$$

where u_γ and φ are the complex representations of the real mechanical displacement and the electric potential, respectively; $C^{(m)}$, $A_\gamma^{(m)}$, and $B^{(m)}$ are determined numerically in the calculating process of SAW velocity on the substrate surface; $\xi = 2\pi/\lambda$ is the wave number; and $p^{(m)}$ is the complex attenuation constant in the x_3-direction.

For the small field perturbation, it can be assumed that $|\tilde{u}_\gamma - u_\gamma| \ll \tilde{u}_\gamma$, $|\tilde{\varphi} - \varphi| \ll \tilde{\varphi}$, and $\tilde{u}_\gamma$ and $\tilde{\varphi}$ are only different from u_γ and φ in the circular frequency of SAW propagation. They can be expressed as

$$\tilde{u}_\gamma = \sum_{m=1}^{4} C^{(m)} A_\gamma^{(m)} e^{\{j[\omega t - \xi(x_1 + p^{(m)} x_3)]\}}, \quad (37)$$

$$\tilde{\varphi} = \sum_{m=1}^{4} C^{(m)} B^{(m)} e^{\{j[\omega t - \xi(x_1 + p^{(m)} x_3)]\}}. \quad (38)$$

In (35)–(38), u_γ, $\tilde{u}_\gamma$, and φ, $\tilde{\varphi}$ are the complex representations of the real mechanical displacement and electric potential, respectively, but we only care about the real part. According to (35)–(38), we can deduce the detailed expression of (34) as follows:

$$\int_{V_0} \tilde{u}_\gamma u_\gamma dV = \int_0^{+\infty} dx_3 \int_{-\frac{\pi}{\xi}}^{\frac{\pi}{\xi}} \tilde{u}_\gamma u_\gamma dx_1 = \frac{2\pi j}{\xi^2} \sum_{m=1}^{4}\sum_{n=1}^{4} \frac{C^{(m)*} A_\gamma^{(m)*} C^{(n)} A_\gamma^{(n)}}{p^{(m)*} - p^{(n)}} = \frac{2\pi j}{\xi^2} E, \quad (39)$$

$$\int_{V_0} \tilde{u}_{a,M} u_{\gamma,L} dV = \int_0^{+\infty} dx_3 \int_{-\frac{\pi}{\xi}}^{\frac{\pi}{\xi}} \tilde{u}_{a,M} u_{\gamma,L} dx_1 = 2\pi j \sum_{m=1}^{4}\sum_{n=1}^{4} \frac{C^{(m)*} A_a^{(m)*} p_M^{(m)*} C^{(n)} A_\gamma^{(n)} p_L^{(n)}}{p^{(m)*} - p^{(n)}} = 2\pi j F, \quad (40)$$

$$\int_{V_0} \tilde{\varphi}_{,M} u_{\gamma,L} dV = \int_0^{+\infty} dx_3 \int_{-\frac{\pi}{\xi}}^{\frac{\pi}{\xi}} \tilde{\varphi}_{,M} u_{\gamma,L} dx_1 = 2\pi j \sum_{m=1}^{4}\sum_{n=1}^{4} \frac{C^{(m)*} B^{(m)*} p_M^{(m)*} C^{(n)} A_\gamma^{(n)} p_L^{(n)}}{p^{(m)*} - p^{(n)}} = 2\pi j G, \quad (41)$$

$$\int_{V_0} \tilde{u}_{a,M}\varphi_{,L} dV = \int_0^{+\infty} dx_3 \int_{-\frac{\pi}{\xi}}^{\frac{\pi}{\xi}} \tilde{u}_{a,M}\varphi_{,L} dx_1 = 2\pi j \sum_{m=1}^{4}\sum_{n=1}^{4} \frac{C^{(m)*} A_a^{(m)*} p_M^{(m)*} C^{(n)} B^{(n)} p_L^{(n)}}{p^{(m)*} - p^{(n)}} = 2\pi j W, \quad (42)$$

$$\int_{V_0} \tilde{\varphi}_{,M}\varphi_{,L} dV = \int_0^{+\infty} dx_3 \int_{-\frac{\pi}{\xi}}^{\frac{\pi}{\xi}} \tilde{\varphi}_{,M}\varphi_{,L} dx_1 = 2\pi j \sum_{m=1}^{4}\sum_{n=1}^{4} \frac{C^{(m)*} B^{(m)*} p_M^{(m)*} C^{(n)} B^{(n)} p_L^{(n)}}{p^{(m)*} - p^{(n)}} = 2\pi j Q, \quad (43)$$

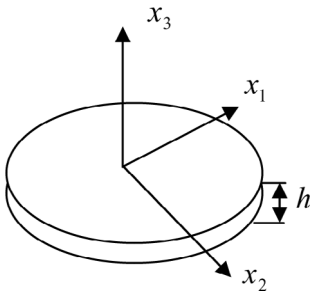

Fig. 1. Circular piezoelectric plate and the reference coordinates.

$$\int_{S_0} \overline{T}_\gamma u_\gamma dS = \int_{-\frac{\pi}{\xi}}^{\frac{\pi}{\xi}} \overline{T}_\gamma u_\gamma dx_1 = 0. \tag{44}$$

From (31), (34), and (39)–(44), the detailed expression of (34) is obtained as

$$\frac{\Delta v}{v_0} = \frac{\hat{c}_{L\gamma Ma} + \hat{e}_{ML\gamma} G + \hat{e}_{LMa} W - \hat{\varepsilon}_{LM} Q}{2\rho^0 v_0^2 E}. \tag{45}$$

Eq. (45) expresses the SAW velocity shift caused by perturbation on the surface of the piezoelectric substrate. In what follows, the problems about the pressure perturbation and the temperature perturbation are analyzed respectively.

To simplify, suppose there is no static biasing electric field in the small field perturbation. Thus, $E_j = 0$. In addition, the third-order electrostrictive, electric permeability, and electroelastic constants are nonlinear constants of piezoelectric substrates, and have been neglected here.

First, let's consider the perturbation from the pressure only. It can be obtained from (7)–(10) as

$$\begin{aligned} \hat{c}_{L\gamma Ma} &= T_{LM}\delta_{\gamma a} + c_{L\gamma MaAB}E_{AB} \\ &\quad + c_{L\gamma KM}\hat{u}_{a,K} + c_{LKMa}\hat{u}_{\gamma,K}, \end{aligned} \tag{46}$$

$$\hat{e}_{ML\gamma} = -e_{MLK}\hat{u}_{\gamma,K}, \tag{47}$$

$$\hat{\varepsilon}_{LM} = -2\varepsilon_0 E_{ML}. \tag{48}$$

Consider a circular piezoelectric plate of thickness h and radius R with a rigidly fixed periphery, which is subjected to pressure P on one of its surfaces. It is shown in Fig. 1.

The static strain tensor components on the surface of the membrane due to the application of pressure P can be calculated according to (8)–(10) in [12], and they are the linear functions of pressure P. The stress tensor components can be obtained from the Hooke law and they also are the linear functions of pressure P. Suppose the primary pressure $P_0 = 0$; this leads to

$$\begin{aligned} \hat{c}_{L\gamma Ma} &= T_{LM}\delta_{\gamma a} + c_{L\gamma MaAB}E_{AB} + c_{L\gamma KM}\hat{u}_{a,K} \\ &\quad + c_{LKMa}\hat{u}_{\gamma,K} \\ &= \hat{c}^P_{L\gamma Ma}(P - P_0) = \hat{c}^P_{L\gamma Ma}\Delta P, \end{aligned} \tag{49}$$

$$\hat{e}_{ML\gamma} = -e_{MLK}\hat{u}_{\gamma,K} = \hat{e}^P_{ML\gamma}(P - P_0) = \hat{e}^P_{ML\gamma}\Delta P, \tag{50}$$

$$\hat{\varepsilon}_{LM} = -2\varepsilon_0 E_{ML} = \hat{\varepsilon}^P_{LM}(P - P_0) = \hat{\varepsilon}^P_{LM}\Delta P. \tag{51}$$

From (49)–(51) and (45), the velocity shift caused by the pressure bias is

$$\begin{aligned} \frac{\Delta v}{v_0 \Delta P} &= \frac{\hat{c}_{L\gamma Ma}F + \hat{e}_{ML\gamma}G + \hat{e}_{LMa}W - \hat{\varepsilon}_{LM}Q}{2\rho^0 v_0^2 E \Delta P} \\ &= \frac{\hat{c}^P_{L\gamma Ma}F + \hat{e}^P_{ML\gamma}G + \hat{e}^P_{LMa}W - \hat{\varepsilon}^P_{LM}Q}{2\rho^0 v_0^2 E}. \end{aligned} \tag{52}$$

Then, consider the perturbation from the temperature only. In this state,

$$\begin{aligned} \hat{c}_{L\gamma Ma} &= T_{LM}\delta_{\gamma a} + c_{L\gamma MaAB}E_{AB} + c_{L\gamma KM}\hat{u}_{a,K} \\ &\quad + c_{LKMa}\hat{u}_{\gamma,K} + \frac{dc_{L\gamma Ma}}{dT}(T - T_0), \end{aligned} \tag{53}$$

$$\hat{e}_{ML\gamma} = -e_{MLK}\hat{u}_{\gamma,K} + \frac{de_{ML\gamma}}{dT}(T - T_0), \tag{54}$$

$$\hat{\varepsilon}_{LM} = -2\varepsilon_0 E_{ML} + \frac{d\varepsilon_{LM}}{dT}(T - T_0). \tag{55}$$

If the substrate expands freely, the stress $T_{LM} = 0$, and the strain is related to the linear expand coefficient α_{AB} by

$$E_{AB} = \alpha_{AB}(T - T_0). \tag{56}$$

According to the free expansion conditions and (56), (53)–(55) can be written as (57)–(59).

$$\begin{aligned} \hat{c}_{L\gamma Ma} &= c_{L\gamma MaAB}\alpha_{AB}(T - T_0) + c_{L\gamma KM}\alpha_{aK}(T - T_0) \\ &\quad + c_{LKMa}\alpha_{\gamma K}(T - T_0) + \frac{dc_{L\gamma Ma}}{dT}(T - T_0) \\ &= \left[c_{L\gamma MaAB}\alpha_{AB} + c_{L\gamma KM}\alpha_{aK} \right. \\ &\quad \left. + c_{LKMa}\alpha_{\gamma K} + \frac{dc_{L\gamma Ma}}{dt}\right](T - T_0) \\ &= \hat{c}^T_{L\gamma Ma}\Delta T, \end{aligned} \tag{57}$$

$$\begin{aligned} \hat{e}_{ML\gamma} &= -e_{MLK}\alpha_{\gamma K}(T - T_0) + \frac{de_{ML\gamma}}{dT}(T - T_0) \\ &= \left(-e_{MLK}\alpha_{\gamma K} + \frac{de_{ML\gamma}}{dT}\right)(T - T_0) \\ &= \hat{e}^T_{ML\gamma}\Delta T, \end{aligned} \tag{58}$$

$$\begin{aligned} \hat{\varepsilon}_{LM} &= -2\varepsilon_0\alpha_{ML}(T - T_0) + \frac{d\varepsilon_{LM}}{dT}(T - T_0) \\ &= \left(-2\varepsilon_0\alpha_{ML} + \frac{d\varepsilon_{LM}}{dT}\right)(T - T_0) = \hat{\varepsilon}^T_{LM}\Delta T. \end{aligned} \tag{59}$$

From (57)–(59) and (45), the velocity shift caused by the temperature bias is

$$\begin{aligned} \frac{\Delta v}{v_0 \Delta T} &= \frac{\hat{c}_{L\gamma Ma}F + \hat{e}_{ML\gamma}G + \hat{e}_{LMa}W - \hat{\varepsilon}_{LM}Q}{2\rho^0 v_0^2 E \Delta T} \\ &= \frac{\hat{c}^T_{L\gamma Ma}F + \hat{e}^T_{ML\gamma}G + \hat{e}^T_{LMa}W - \hat{\varepsilon}^T_{LM}Q}{2\rho^0 v_0^2 E}. \end{aligned} \tag{60}$$

III. Pressure and Temperature Coefficients

For the pressure and temperature sensors based on SAW resonators, the SAW wavelength λ is considered a constant. The relationship between the resonant frequency

shift of the SAW resonator and the variances of the pressure and temperature can be written as

$$\begin{aligned}\frac{df}{f} &= \frac{dv}{v} = \frac{1}{v}\frac{\partial v}{\partial P}dP + \frac{1}{v}\frac{\partial v}{\partial T}dT \\ &\approx \frac{1}{v}\frac{\Delta v}{\Delta P}dP + \frac{1}{v}\frac{\Delta v}{\Delta T}dT = \alpha_P^R dP + \alpha_T^R dT. \end{aligned} \quad (61)$$

In (61), f is the resonant frequency, and α_P^R and α_T^R are the pressure and temperature coefficients of frequency on piezoelectric substrates, respectively.

For the pressure and temperature sensors based on SAW delay lines, the SAW frequency can be considered as a constant f_0. The relationship between the delay time or phase shift of the SAW delay line and the variances of the pressure and temperature can be obtained as

$$\begin{aligned}\frac{d\phi}{\phi} &= \frac{d(2\pi f_0 \tau)}{2\pi f_0 \tau} = \frac{d\tau}{\tau} = \frac{d(l/v)}{l/v} = \frac{dl}{l} - \frac{dv}{v} \\ &= \left(\frac{1}{l}\frac{\partial l}{\partial P} - \frac{1}{v}\frac{\partial v}{\partial P}\right)dP + \left(\frac{1}{l}\frac{\partial l}{\partial T} - \frac{1}{v}\frac{\partial v}{\partial T}\right)dT \\ &= \left(s_{11} - \frac{1}{v}\frac{\partial v}{\partial P}\right)dP + \left(\alpha_{11} - \frac{1}{v}\frac{\partial v}{\partial T}\right)dT \\ &\approx \left(s_{11} - \frac{1}{v}\frac{\Delta v}{\Delta P}\right)dP + \left(\alpha_{11} - \frac{1}{v}\frac{\Delta v}{\Delta T}\right)dT \\ &= \alpha_P^D dP + \alpha_T^D dT. \end{aligned} \quad (62)$$

In (62), ϕ is the delay phase of the SAW delay line, τ is the delay time of the SAW delay line, l is the length that the SAW propagates along the substrate surface, s_{11} and α_{11} are the elastic compliance constants and the thermal expansion constant of the substrate, respectively, in the direction of SAW propagation, and α_P^D and α_T^D are the pressure and temperature coefficients of delay on the substrate, respectively.

IV. Effective SAW Coupling Coefficient, PFA and Acoustic Propagation Loss

The effective SAW coupling coefficient is defined as the electromechanical coupling constant of the substrate that denotes the efficiency of electromechanical transformation. For SAW sensors, the substrate that has an effective SAW coupling coefficient as large as possible should be selected. It can be calculated according to [16].

The PFA is the angle between the direction of energy propagation and the direction of the SAW propagation in the substrate surface. Because the direction of SAW energy propagation is not usually the same as the direction of SAW propagation, the PFA is not zero in most cases. For SAW sensors, the substrate that has the PFA as small as possible should be selected. In this case, the direction of energy propagation is close to the direction of the SAW propagation and the energy can be used fully. The PFA can be calculated according to [16].

The acoustic propagation loss is the amplitude decay of the acoustic wave due to material damping; scattering caused by defects, surface finish, or electrodes; and acoustic bulk-wave radiation into the ambient environment. Specifically, this is the ratio of the power transmitted in a SAW beam to the power received, expressed in dB.

V. Objective Function

In Sections III–IV, we analyzed the pressure coefficient, the temperature coefficient, the effective SAW coupling coefficient, the PFA, and the acoustic propagation loss. They have different values for the different piezoelectric substrates and crystal cuts. In order to select the optimized substrate and crystal cut, we should consider all of these factors synthetically.

The basic requirements for piezoelectric substrates of SAW-based pressure and temperature sensors are as follows:

- The pressure coefficient should be as large as possible for piezoelectric substrates of SAW-based pressure sensors and should be as small as possible for piezoelectric substrates of SAW-based temperature sensors.
- The temperature coefficient should be as small as possible for piezoelectric substrates of SAW-based pressure sensors and should be as large as possible for piezoelectric substrates of SAW-based temperature sensors.
- The effective SAW coupling coefficient should be as large as possible.
- The PFA should be as small as possible. It is usually not allowed to be in excess of the range of $(-5^\circ, 5^\circ)$.
- The acoustic propagation loss should be as small as possible.

In order to meet the requirements above, we define the objective function as

$$\begin{aligned} &\max F(\theta,\phi,\psi) = (-1)^{a_1}\frac{\alpha_P}{\alpha_{P_{\max}}} \times (-1)^{a_2}\frac{|\alpha_T|}{\alpha_{T_{\max}}}, \\ &s.t.\ \ K^2 \geq K, \\ &\qquad PFA \leq 5^\circ, \\ &\qquad \theta,\phi,\psi \in [-90^\circ, 90^\circ], \end{aligned} \quad (63)$$

where α_P and α_T are the pressure and temperature coefficients of piezoelectric substrates, respectively; $\alpha_{P_{\max}}$ and $\alpha_{T_{\max}}$ are the maximum pressure and temperature coefficients, respectively; α_P and α_T should be the pressure and temperature coefficients of frequency α_P^R and α_T^R, respectively, for piezoelectric substrates of pressure and temperature sensors based on SAW resonators; α_P and α_T should be the pressure and temperature coefficients of delay α_P^D and α_T^D, respectively, for piezoelectric substrates of pressure and temperature sensors based on SAW delay lines; a_1 and a_2 are the linear coefficients; $a_1 = 0$ and $a_2 = 1$ for piezoelectric substrates of SAW-based pressure sensors; $a_1 = 1$ and $a_2 = 0$ for piezoelectric substrates of SAW-based temperature sensors; $a_1 = 0$ and $a_2 = 0$ for piezoelectric substrates of SAW-based pressure/temperature sensors; and K is the minimum of the

effective SAW coupling coefficient for the selection requirement. Because the acoustic propagation loss is not easy to obtain, we did not consider it in this function.

In terms of pressure coefficients, temperature coefficients, effective SAW coupling coefficients, and PFAs of the piezoelectric substrates with different cut angles, we can obtain the optimal selections for SAW-based pressure and temperature sensors by searching the maximum of (63).

VI. Numerical Results

From the objective function defined in Section V, we can achieve the optimal selection of piezoelectric substrates and crystal cuts for SAW-based pressure and temperature sensors. But the optimal selection is not global optimization because there are many substrate materials for which we do not know the parameters. So it should be an optimization in a special range.

Quartz, $LiNbO_3$, and $LiTaO_3$ crystals are widely used as piezoelectric substrates for SAW-based pressure and temperature sensors. The crystal cuts can be expressed with the Euler angle (θ, ϕ, ψ) which reflects the rotation angles from the crystal axis (X, Y, Z) to the substrate coordinate axis (x, y, z). In most cases, the crystal is X-cut, Y-cut, Z-cut, and rotated Y-cut. In other words, (90°,90°,ψ), (0°,90°,ψ), (0°,0°,ψ), and (0°,ϕ,0°) represent the X-cut, Y-cut, Z-cut, and rotated Y-cut, respectively.

In this paper, we calculated the SAW velocities in different propagation directions of X-cut, Y-cut, Z-cut, and rotated Y-cut quartz, $LiNbO_3$, and $LiTaO_3$ crystals using the material constants from [17]–[23]. The SAW velocity was solved with the mixed method of surface effective permittivity and boundary condition determinant mentioned in [24]. Using [16], we calculated their effective SAW coupling coefficients and PFAs. Using (39)–(62), we computed their pressure and temperature coefficients of frequency and their pressure and temperature coefficients of delay.

In order to verify the correctness of our calculations, we compared our data with [9] for temperature coefficients of frequency of X-cut, Y-cut, and rotated Y-cut quartz. The results are shown in Figs. 2–4. The dashed curve shows the average of the calculated values at 0°C and 50°C from [9]. The triangles are the average of the experimental values from [9]. The solid curve shows our calculated values. It can be seen that our data fit the experimental results well.

We also compared our results with [21] for temperature coefficients of delay of X-cut $LiTaO_3$. The results are shown in Fig. 5. The dotted curve shows the Smith and Welsh calculated values from [21]. The dot and dash curve shows the Kozlov calculated values from [21]. The triangles are the experimental values from [21]. The solid curve shows our calculated values. It can be seen that our data agree well with the experimental data.

According to the computed results of the effective SAW coupling coefficients, the PFAs, the pressure and temperature coefficients of frequency, and the pressure and temperature coefficients of delay of the three substrates,

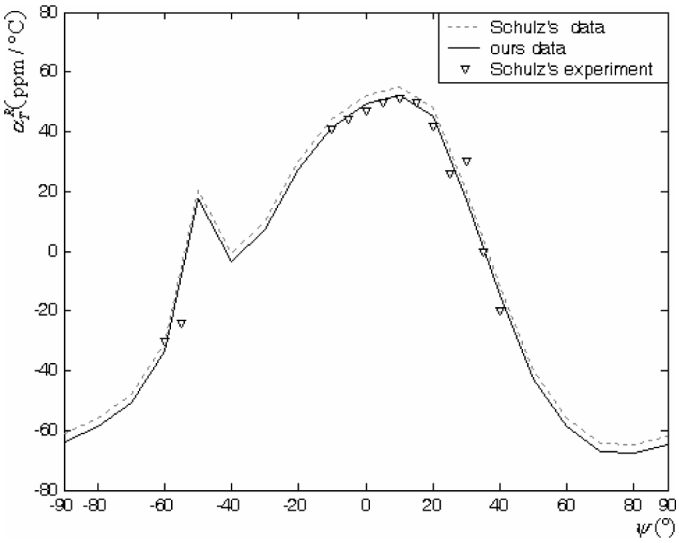

Fig. 2. Calculated and measured values of temperature coefficients of frequency as a function of the SAW propagation direction of X-cut quartz.

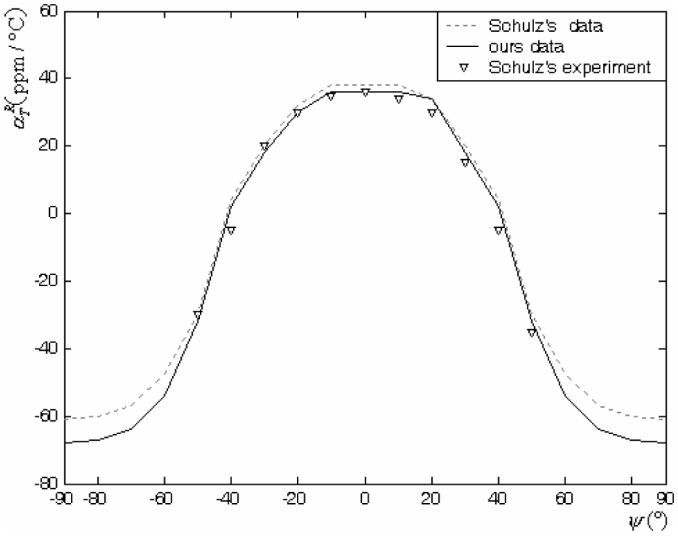

Fig. 3. Calculated and measured values of temperature coefficients of frequency as a function of the SAW propagation direction of Y-cut quartz.

we calculated the maximum of (63) for piezoelectric substrates of pressure sensors, temperature sensors, and pressure/temperature sensors based on SAW resonators and SAW delay lines, and achieved their optimal selections of substrates and crystal cuts.

For pressure sensors based on SAW resonators, rotated Y-cut 42° quartz substrate is the optimal selection. The selection is near the ST, X-cut quartz. Its Euler angle is (0°, 42°, 0°). The corresponding SAW velocity in the free surface is 3165.63 m/s. The effective SAW coupling coefficient is 0.0922%. PFA is −0.598°. The pressure coefficient of frequency is 54.465 ppm/Pa. The temperature coefficient of frequency is 13.395 ppm/°C.

For temperature sensors based on SAW resonators, rotated Y-cut 38° $LiNbO_3$ substrate is the optimal se-

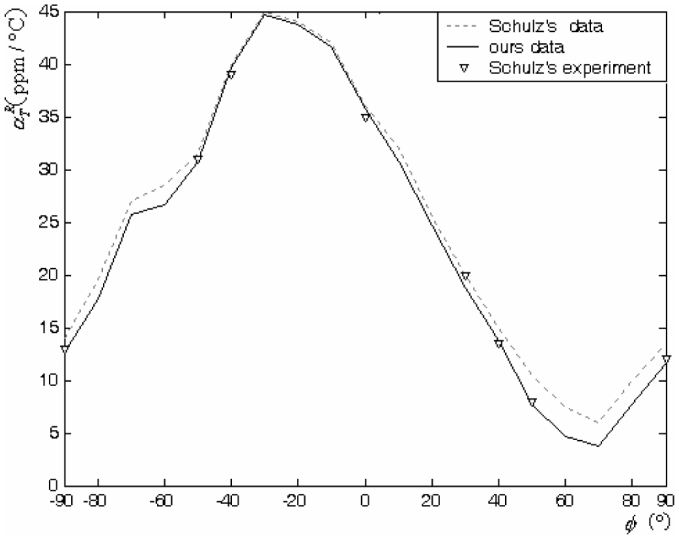

Fig. 4. Calculated and measured values of temperature coefficients of frequency as a function of the SAW propagation direction of rotated Y-cut quartz.

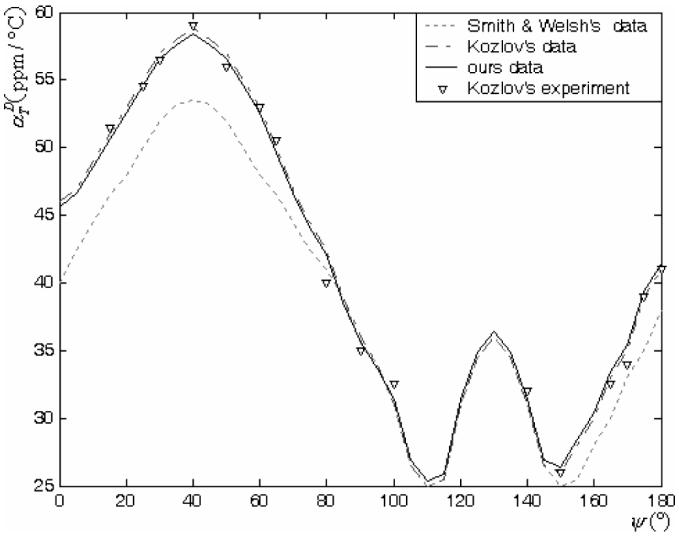

Fig. 5. Calculated and measured values of temperature coefficients of delay as a function of the SAW propagation direction of X-cut $LiTaO_3$.

lection here, which is the same as the selection of the 128° YX-$LiNbO_3$ in [16]. Its Euler angle is (0°, 38°, 0°). The corresponding SAW velocity in the free surface is 3976.38 m/s. The effective SAW coupling coefficient is 4.33%. PFA is 1.1281°. The pressure coefficient of frequency is 5.671 ppm/Pa. The temperature coefficient of frequency is 68.52 ppm/°C.

For pressure/temperature sensors based on SAW resonators, Y-cut 35° quartz substrate is the optimal selection. Its Euler angle is (0°, 90°, 35°). The corresponding SAW velocity in the free surface is 3642.11 m/s. The effective SAW coupling coefficient is 0.12%. PFA is −3.1575°. The pressure coefficient of frequency is 22.661 ppm/Pa. The temperature coefficient of frequency is 16.61 ppm/°C.

For pressure sensors based on SAW delay lines, rotated Y-cut 40° quartz substrate is the optimal selection. Its Euler angle is (0°, 40°, 0°). The corresponding SAW velocity in the free surface is 3168.14 m/s. The effective SAW coupling coefficient is 0.12%. PFA is −0.6217°. The pressure coefficient of delay is 56.815 ppm/Pa. The temperature coefficient of delay is 8.7020 ppm/°C.

For temperature sensors based on SAW delay lines, Y-cut 90° $LiNbO_3$ substrate is the optimal selection. Its Euler angle is (0°, 90°, 90°). The corresponding SAW velocity in the free surface is 3497.27 m/s. The effective SAW coupling coefficient is 5.03%. PFA is 0.3849°. The pressure coefficient of delay is 26.2175 ppm/Pa. The temperature coefficient of delay is −74.79 ppm/°C.

For pressure/temperature sensors based on SAW delay lines, Y-cut quartz substrate is the optimal selection. Its Euler angle is (0°, 90°, 0°). The corresponding SAW velocity in the free surface is 3447.61 m/s. The effective SAW coupling coefficient is 0.095%. PFA is −0.5903°. The pressure coefficient of delay is 28.971 ppm/Pa. The temperature coefficient of delay is −25.79 ppm/°C.

VII. Conclusion

The selection of piezoelectric substrates and crystal cuts is an important problem of SAW-based pressure/temperature sensor design. Optimizing the selection in order to obtain the optimal measurement performance is discussed in this paper.

Especially, the optimal selections among the range of X-cut, Y-cut, Z-cut, and rotated Y-cut quartz, $LiNbO_3$, and $LiTaO_3$ crystals are achieved in this paper. And the optimal selections among the range of XY-cut, YZ-cut and ZX-cut quartz, $LiNbO_3$, $LiTaO_3$, and other new crystals can be obtained by using almost the same method proposed here. Further experimental verifications of the proposed method are in progress. Regarding trends proposed in [25], [26], the means of incorporating the measurements of SAW sensors into tire dynamic models is also under careful consideration.

References

[1] X. Zhang, Z. Wang, L. Gai, Y. Ai, and F. Wang, "Design considerations on intelligent tires utilizing wireless passive surface acoustic wave sensors," in *Proc. 5th World Congress on Intelligent Control and Automation*, 2004, pp. 3696–3670.

[2] F.-Y. Wang, G.-L. Shan, L. Li, Z.-Y. Wang, and C.-Z. Wang, "The research of smart tire and correlative core techniques," *Tire Industry Sinica*, vol. 22, no. 12, pp. 713–719, 2002.

[3] F.-Y. Wang, Z.-X. Wang, G.-L. Shan, L. Li, and C.-Z. Wang, "Study progress and prospect of smart tire," *Rubber Industry Sinica*, vol. 23, no. 1, pp. 10–15, 2003.

[4] A. Pohl, G. Ostermayer, L. Reindl, and F. Seifert, "Monitoring the tire pressure at cars using passive SAW sensors," in *Proc. IEEE Ultrason. Symp.*, 1997, pp. 471–474.

[5] A. Pohl and F. Seifert, "Wirelessly interrogable surface acoustic wave sensors for vehicular applications," *IEEE Trans. Instrum. Meas.*, vol. 46, no. 4, pp. 1031–1038, 1997.

[6] W. Buff, M. Rusko, T. Vandahl, M. Goroll, and F. Moller, "A differential measurement SAW device for passive remote sensoring," in *Proc. IEEE Ultrason. Symp.*, vol. 1, 1996, pp. 343–346.
[7] W. Buff, M. Rusko, M. Goroll, J. Ehrenpfordt, and T. Vandahl, "Universal pressure and temperature SAW sensor for wireless applications," in *Proc. IEEE Ultrason. Symp.*, vol. 1, 1997, pp. 359–362.
[8] R. Steindle, A. Pohl, L. Reindl, and F. Seifert, "SAW delay lines for wirelessly requestable conventional sensors," in *Proc. IEEE Ultrason. Symp.*, vol. 1, 1998, pp. 351–354.
[9] M. B. Schulz, B. J. Matsinger, and M. G. Holland, "Temperature dependence of surface acoustic wave velocity on α-quartz," *J. Appl. Phys.*, vol. 41, no. 7, pp. 2755–2765, 1970.
[10] B. K. Sinha and H. F. Tiersten, "On the temperature dependence of the velocity of surface waves in quartz," *J. Appl. Phys.*, vol. 51, no. 9, pp. 4659–4664, 1980.
[11] S. Ballandras and E. Bigler, "Surface-acoustic-wave devices with low sensitivity to mechanical and thermoelastic stresses," *J. Appl. Phys.*, vol. 72, no. 8, pp. 3272–3281, 1992.
[12] R. M. Taziev, E. A. Kolosovsky, and A. S. Kozlov, "Pressure-sensitive cuts for surface acoustic waves in α-quartz," *IEEE Trans. Ultrason., Ferroelect., Freq. Contr.*, vol. 42, no. 5, pp. 845–849, 1995.
[13] W. Ma and W. Shi, "Temperature-sensitive cuts for surface acoustic waves in quartz," *IEEE Trans. Ultrason., Ferroelect., Freq. Contr.*, vol. 48, no. 1, pp. 333–335, 2001.
[14] H. F. Tiersten, "Perturbation theory for linear electroelastic equations for small fields superposed on a bias," *J. Acoust. Soc. Amer.*, vol. 64, no. 3, pp. 832–837, 1978.
[15] B. K. Sinha and H. F. Tiersten, "On the influence of a flexural biasing state on the velocity of piezoelectric surface waves," *Wave Motion*, no. 1, pp. 37–51, 1979.
[16] K.-Y. Hashimoto, *Surface Acoustic Wave Devices in Telecommunications Modelling and Simulation*. Berlin, Heidelberg: Springer-Velag, 2000.
[17] R. W. Ward, "The constants of alpha quartz," in *Proc. Int. IEEE Freq. Contr. Symp.*, 1984, pp. 22–31.
[18] R. T. Smith and F. S. Welsh, "Temperature dependence of the elastic, piezoelectric and dielectric constants of lithium tantalate and lithium niobate," *J. Appl. Phys.*, vol. 42, no. 6, pp. 2219–2230, 1971.
[19] R. Brendel, "Material nonlinear piezoelectric coefficients for quartz," *J. Appl. Phys.*, vol. 54, no. 9, pp. 5339–5346, 1983.
[20] Y. Nakagawa, K. Yamanouchi, and K. Shibayama, "Third-order elastic constants of lithium niobate," *J. Appl. Phys.*, vol. 44, no. 9, pp. 3969–3974, 1973.
[21] A. S. Kozlov, R. M. Taziev, I. L. Vasiliev, and I. B. Yakovkin, "Temperature derivatives of elastic stiffness evaluated from the SAW delay-temperature behavior on lithium tantalate plates," in *Proc. IEEE Ultrason. Symp.*, 1995, pp. 393–396.
[22] R. M. Taziev, A. S. Kozlov, I. L. Vasiliev, and I. B. Yakovkin, "Temperature coefficients of first and second orders of elastic stiffness evaluated from the SAW delay-temperature behavior on lithium tantalate plates," in *Proc. IEEE Int. Freq. Contr. Symp.*, 1997, pp. 867–872.
[23] Y.-K. Yong and W. Wei, "Lagrangean temperature coefficients of the piezoelectric stress constants and dielectric permittivity of quartz," in *Proc. IEEE/EIA Int. Freq. Contr. Symp. Exhibit.*, 2000, pp. 364–372.
[24] L.-E. Li, X.-J. Ji, W.-K. Shi, and G.-W. Zhang, "Strategy for the fast solving of surface acoustic waves velocity," *J. Shanghai Jiaotong Univ.*, vol. 39, no. 4, pp. 656–660, 2005.
[25] L. Li, J. Song, F.-Y. Wang, W. Niehsen, and N.-N. Zheng, "New developments and research trends for intelligent vehicles," *IEEE Intell. Syst.*, vol. 20, no. 4, pp. 10–14, 2005.
[26] L. Li, F.-Y. Wang, and Q. Zhou, "Integrated longitudinal and lateral tire/road friction modeling and monitoring for vehicle motion control," *IEEE Trans. Intell. Transport. Syst.*, vol. 7, no. 1, pp. 1–19, 2006.

Xiangwen Zhang received his M.S. degree in control theory and control engineering from Jiaozuo Institute of Technology, Henan, China, in 2002, and his Ph.D. degree in control theory and control engineering from the Institute of Automation, Chinese Academy of Sciences, Beijing, China, in 2005. Since July 2005 he has been with the Department of Computer Science and Technology, Guilin University of Electronic Technology, Guilin, China. His current research interests include SAW sensors and their applications to intelligent tires and automobile electronics.

Fei-Yue Wang (S'87–M'89–SM'94–F'03) received his B.S. degree in chemical engineering from Qingdao University of Science and Technology, Qingdao, China, his M.S. degree in mechanics from Zhejiang University, Hangzhou, China, and his Ph.D. degree in electrical, computer and systems engineering from the Rensselaer Polytechnic Institute, Troy, New York, in 1982, 1984, and 1990, respectively. He joined the University of Arizona in 1990, became a Full Professor of Systems and Industrial Engineering in 1999, and currently is the Director of the Program in Advanced Research for Complex Systems. In 1999, he founded the Intelligent Control and Systems Engineering Center at the Institute of Automation, Chinese Academy of Sciences, Beijing, China, under the support of the Outstanding Oversea Chinese Talents Program. Since 2002 he has been the Director of the Key Laboratory of Complex Systems and Intelligence Science at the Chinese Academy of Sciences.

His current research interests include modeling, analysis, and control mechanism of complex systems; agent-based control systems; intelligent control systems; real-time embedded systems, application-specific operating systems (ASOS); applications in intelligent transportation systems, intelligent vehicles and telematics, web caching and service caching, smart appliances, and home systems; and network-based automation systems. He has published more than 200 books, book chapters, and papers in those areas since 1984 and received more than $20M USD and over ¥50M RMB in grant funding from NSF, DOE, DOT, NNSF, CAS, MOST, Caterpillar, IBM, HP, AT&T, GM, BHP, RVSI, ABB, and Kelon. He received the Caterpillar Research Invention Award with Dr. P. J. A. Lever in 1996 for his work in robotic excavation, and the National Outstanding Young Scientist Research Award from the National Natural Science Foundation of China in 2001, as well as various industrial awards from major corporations for his applied research. He was the Editor-in-Chief of the International Journal of Intelligent Control and Systems from 1995 to 2000, was Editor-in-Charge of Series in Intelligent Control and Intelligent Automation from 1996 to 2004, and currently is the Editor-in-Charge of Series in Complex Systems and Intelligence Science, an Associate Editor and the Editor for the Intelligent Transportation Systems Department of the IEEE Intelligent Systems, and an Associate Editor of the IEEE Transactions on Systems, Man, and Cybernetics, IEEE Transactions on Robotics and Automation, IEEE Transactions on Intelligent Transportation Systems, and several other international journals. He is an elected member of IEEE SMC Board of Governors and the AdCom of the IEEE Nanotechnology Council, the President-Elect of IEEE Intelligent Transportation Systems Society, and Chair of the Technical Committee on System Complexity of the Chinese Association of Automation. He was the Program Chair of the 1998 IEEE Int'l Symposium on Intelligent Control and the 2001 IEEE Int'l. Conference on Systems, Man, and Cybernetics, Chair for Workshops

and Tutorials for 2002 IEEE Int'l. Conference on Decision and Control (CDC), the General Chair of the 2003 IEEE Int'l. Conference on Intelligent Transportation Systems, and Co-Program Chair of the 2004 IEEE Int'l. Symposium on Intelligent Vehicles and the General Chair for the same conference in 2005, the General Chair of the IEEE 2005 International Conference on Networking, Sensing, and Control, ASME/IEEE Int'l. Conference on Mechatronic/Embedded Systems and Applications, and Program Chair of IEEE Int'l Conference on Vehicular Electronics and Safety. He was the Vice President and one of the major contributors of the American Zhu Kezhen Education Foundation, and a member of the Boards of Directors of five companies in information technology and automation. Dr. Wang is also a member of Sigma Xi, ACM, AMSE, ASEE, and the International Council of Systems Engineering (INCOSE).

Li Li (S'05–M'06) received his B.S. degree in electronics and information engineering from Huazhong University of Science and Technology, Wuhan, China, in 1999, his M.S. degree in industrial engineering from the University of Arizona, Tucson, in 2003, and his Ph.D. degree in systems engineering from the same university in 2005. He is currently an assistant professor at the Department of Automation, Tsinghua University, working in the fields of intelligent control and sensory, intelligent vehicles, and intelligent transportation systems.